Multigap Superconductivity and Strong Electron-Boson Coupling in Fe-Based Superconductors: A Point-Contact Andreev-Reflection Study of $Ba(Fe_{1-x}Co_x)_2As_2$ Single Crystals

M. Tortello,[1] D. Daghero,[1] G. A. Ummarino,[1] V. A. Stepanov,[2] J. Jiang,[3] J. D. Weiss,[3] E. E. Hellstrom,[3] and R. S. Gonnelli[1,*]

[1]*Dipartimento di Fisica, Politecnico di Torino, 10129 Torino, Italy*
[2]*P. N. Lebedev Physical Institute, Russian Academy of Sciences, 119991 Moscow, Russia*
[3]*Applied Superconductivity Center, National High Magnetic Field Laboratory, Florida State University, Tallahassee, Florida 32310, USA*

(Received 4 August 2010; published 2 December 2010)

Directional point-contact Andreev-reflection measurements in $Ba(Fe_{1-x}Co_x)_2As_2$ single crystals (T_c = 24.5 K) indicate the presence of two superconducting gaps with no line nodes on the Fermi surface. The point-contact Andreev-reflection spectra also feature additional structures related to the electron-boson interaction, from which the characteristic boson energy $\Omega_b(T)$ is obtained, very similar to the spin-resonance energy observed in neutron scattering experiments. Both the gaps and the additional structures can be reproduced within a three-band $s\pm$ Eliashberg model by using an electron-boson spectral function peaked at $\Omega_0 = 12$ meV $\simeq \Omega_b(0)$.

DOI: 10.1103/PhysRevLett.105.237002 PACS numbers: 74.50.+r, 74.45.+c, 74.70.Dd

The discovery of the first class of noncuprate, Fe-based high-temperature superconductors in 2008 brought great excitement in the scientific community [1]. The phase diagram of these compounds (although still imperfectly known) looks similar to that of copper-oxide superconductors [2,3], and, as in cuprates, superconductivity emerges ''in the vicinity'' of a magnetic parent compound. The electron-phonon interaction seems not to be sufficient [4] to explain their high T_c (up to 55 K [5]) even if a magnetic ground state is considered [6]. A pairing mechanism involving spin fluctuations (SFs) has been early proposed instead, which predicts the occurrence of a sign change of the order parameter on different sheets of the Fermi surface (FS) [7]. This so-called $s\pm$ model is strongly supported by various experimental results [8] which show multiple nodeless gaps on different sheets of the FS, although the possible emergence of gap nodes in particular cases [9,10] is still debated. The role of SFs in the pairing has also found support in neutron scattering experiments that have revealed a spin resonance whose energy scales linearly with T_c [2]. Finally, it has been recently shown that a multiband $s\pm$ Eliashberg model can reproduce several experimental quantities (such as gaps, T_c, kinks in the band dispersion, and effective masses [11,12]) by assuming that the mediating boson has a characteristic energy similar to the spin-resonance one.

In this Letter, we report on *directional* point-contact Andreev-reflection (PCAR) measurements on high-quality single crystals of the *e*-doped 122 compound $BaFe_{1.8}Co_{0.2}As_2$. The results prove the existence of two superconducting gaps with no line nodes on the FS and whose amplitude is almost the same in the *ab* plane or along the *c* axis. The PCAR spectra also present structures that can be related to a strong electron-boson interaction (EBI). The characteristic energy Ω_b of the mediating boson extracted from the PCAR curves decreases with temperature and is very similar to the resonance energy of the spin excitation spectrum [13]. Moreover, both the gaps and the additional EBI structures in the PCAR spectra can be reproduced within an effective three-band $s\pm$ wave Eliashberg model using a boson energy $\Omega_0 = 12$ meV $\simeq \Omega_b(0)$. All these results strongly support a spin-fluctuation-mediated mechanism for superconductivity in this compound.

The $BaFe_{1.8}Co_{0.2}As_2$ single crystals were prepared by the self-flux method [14] under a pressure of 280 MPa at the National High Magnetic Field Laboratory in Tallahassee. The typical crystal size is $\approx 1 \times 1 \times 0.1$ mm^3. The onset of the resistive transition is $T_c^{\text{on}} = 24.5$ K with ΔT_c (10%–90%) = 1 K (see the inset in Fig. 1). Instead of using the standard technique where a sharp metallic tip is pressed against the material under study, the point contacts were made by putting a small drop of Ag paste on a fresh surface exposed by breaking the crystal. The setup for PCAR measurements with current injection along the *c* axis and along the *ab* plane is shown in Fig. 2(a) and 2(d), respectively. Contacts made in this way are very stable, and their differential conductance $G_{\text{exp}}(V) = dI(V)/dV$ can be recorded up to ≈ 200 K [15]. As an example, Fig. 1 shows the raw conductance curves (up to 180 K) of a $Ag/BaFe_{1.8}Co_{0.2}As_2$ point contact ($R_N = 25\ \Omega$) with current injection along the *c* axis (''*c*-axis contact''). The clear signatures of AR in the low-*T* curve and the absence of heating effects or dips [16] indicate that the conduction through the contact is ballistic and energy-resolved spectroscopy is possible. At a closer inspection the maxima in the low-*T* curves reveal fine structures (indicated by arrows in Fig. 1) suggesting

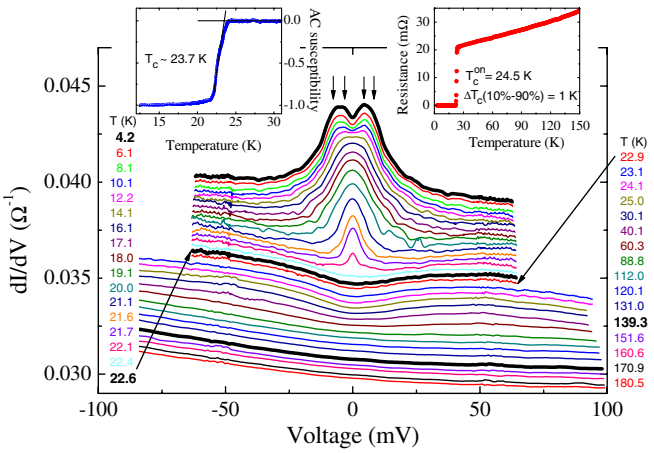

FIG. 1 (color online). Temperature dependence of the conductance curves in a $Ag/BaFe_{1.8}Co_{0.2}As_2$ c-axis point contact. The curves are vertically offset for clarity. The insets show the superconducting transition as seen by ac magnetic susceptibility (left) and dc resistance (right) measurements.

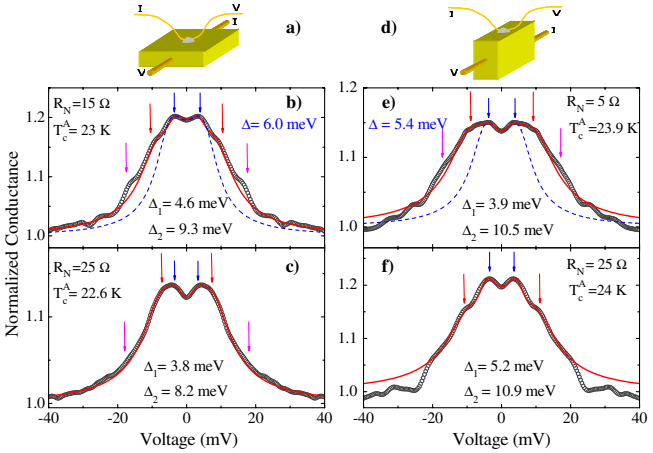

FIG. 2 (color online). (a),(d) Sketch of c-axis and ab-plane contacts. (b),(c) Normalized conductance curves at 4.2 K for c-axis contacts (symbols) and their two-band fit (solid lines) with the relevant gap values Δ_1 and Δ_2. Arrows mark the structures related to the gaps and to the EBI. (e),(f) The same for two ab-plane contacts. In (b) and (e), a single-band fit is also shown (dashed lines) with the relevant gap amplitude Δ.

multiple gaps. The Andreev signal decreases on increasing T and vanishes at the critical temperature of the contact, $T_c^A = 22.6 \pm 0.2$ K, leaving a slightly V-shaped normal state. On further heating, the normal-state curve progressively fills and completely flattens at ≈ 140 K, the temperature where the long-range magnetic order sets in in the parent compound. Similar behavior was observed in 1111 Fe-based superconductors [15,17].

In order to compare the experimental curves to a suitable model, all the raw conductance curves $G_{\rm exp}(V)$ at $T < T_c^A$ were first normalized (i.e., divided by the normal-state curve at T_c^A) and then symmetrized so as to get rid of the well-known asymmetry of the PCAR spectra of Fe-based compounds [15,17,18] though preserving and enhancing the structures we are interested in (gaps and EBI). The resulting conductance curves were fitted to a two-band [19] Blonder-Tinkham-Klapwijk (BTK) model taking into account broadening effects and the angular distribution of the injected current [16]. In this model the normalized conductance $G(V)$ is the weighed sum of two BTK terms: $G(V) = w_1 G_1(V) + (1 - w_1) G_2(V)$, where w_1 is the weight of contribution 1. Each $G_i(V)$ is described by a gap Δ_i, a broadening parameter Γ_i (here mostly due to inelastic scattering in the vicinity of the contact), and a parameter Z_i which accounts for the height of the potential barrier at the N/S interface and the Fermi velocity mismatch [16].

Examples of normalized conductance curves at 4.2 K are shown in Figs. 2(b) and 2(c) for c-axis contacts and in 2(e) and 2(f) for ab-plane contacts. All the PCAR spectra show peaks at ≈ 4 meV and shoulders at ≈ 9–10 meV. Additional structures are reproducibly present at 18–20 mV, although more pronounced when the Andreev signal is higher. In a few cases [Fig. 2(f)] they are masked by small dips, which however do not affect the very clear two-gap structures at lower energy. Figures 2(b) and 2(e) and the inset to Fig. 3 clearly show that, while the one-gap BTK model (dashed lines) is unsuited to reproduce the experimental curves, the two-gap BTK model (solid lines) fits the data rather well (apart from the structures around 20 mV). The resulting amplitudes of the gaps Δ_1 and Δ_2 are indicated in the labels. In all the two-gap fits of this Letter, $w_1 = 0.5 \pm 0.1$ and, at low T, $\Gamma/\Delta = 0.5$–0.7. Finally, Z and w_1 are constant with temperature while Γ is almost constant or slightly increases with T [15,16]. From the fits of various curves we obtained the average values $\Delta_1^c = 4.1 \pm 0.4$ meV and $\Delta_2^c = 9.2 \pm 1.0$ meV for

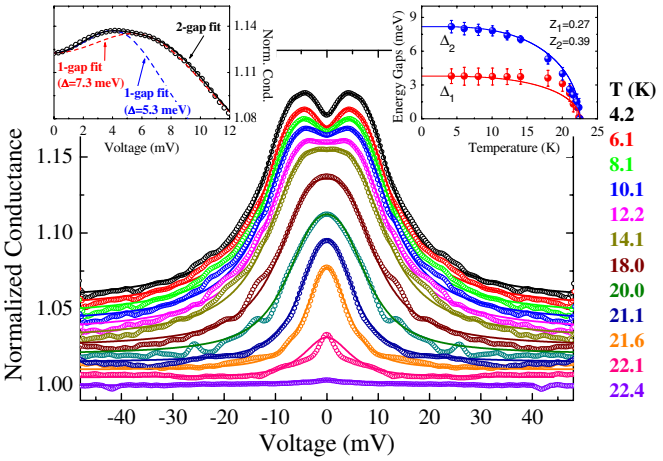

FIG. 3 (color online). Temperature dependence of the normalized conductance of Fig. 2(c) (symbols) and the relevant two-band BTK fits (lines). All curves except the bottom one are offset for clarity. Right inset: The gaps given by the fit (symbols) and the BCS-like temperature dependencies (lines). Left inset: Zoom of the curve at 4.2 K (symbols) with two possible one-gap BTK fits (dashed lines) and the best two-band BTK fit (solid line).

c-axis spectra and $\Delta_1^{ab} = 4.4 \pm 0.6$ meV and $\Delta_2^{ab} = 9.9 \pm 1.2$ meV for ab-plane contacts. These results can be compared to angle-resolved photoemission spectroscopy (ARPES) experiments [20], which show two nodeless gaps in the $k_x k_y$ plane. The small gap, located on one of the electron FS sheets, is in very good agreement with our Δ_1. Our value of Δ_2 is instead about 30% bigger than the large ARPES gap, located on the hole FS sheet. The reason of this discrepancy will become clear in the following. In this concern, note that, although directional PCAR measurements are not k-resolved, they allow probing the gaps also along the $\mathbf{k}_z$ direction, not easily accessible to ARPES measurements.

The absence of zero-bias conductance peaks in the PCAR spectra along either direction rules out line nodes on the FS but does not exclude deep gap minima or even zeros in small regions of the Brillouin zone [10,21,22]. The fact that w_1 is almost independent of the direction suggests an almost equal degree of three-dimensionality of the various FS sheets in $Ba(Fe_{1-x}Co_x)_2As_2$, as also shown by ARPES [23], x-ray Compton scattering [24], and first-principles calculations [21,25].

Figure 3 shows the temperature dependence of the normalized conductance of Fig. 2(c) (symbols) and the relevant two-band BTK fit (lines). The two-band model fits very well the low-T spectrum (see the left inset) giving $\Delta_1(0) = 3.8$ meV and $\Delta_2(0) = 8.2$ meV, which correspond to $2\Delta_1/k_B T_c \approx 3.9$ and $2\Delta_2/k_B T_c \approx 8.5$, both above the BCS weak-coupling ratio. The temperature dependence of the gaps is shown in the right inset (symbols).

It has been recently shown that in La-1111, Sm-1111, and $Ba_{1-x}K_xFe_2As_2$ the experimental gap values and their temperature dependence can be reproduced within a three-band $s\pm$ Eliashberg model [11,12], while two- or three-band weak-coupling BCS models cannot do the same. In $Ba(Fe_{0.9}Co_{0.1})_2As_2$ we can simplify the electronic structure, according to ARPES measurements [20], by taking one effective hole band (band 1) and two electron ones (bands 2 and 3, corresponding to the outer and inner electron barrels in the FS as defined in Ref. [21]). We disregard the small hole pocket at Γ, predicted by calculations but not observed by ARPES. Phonons mainly provide intraband coupling, but their contribution is expected to be small [4,6], while SFs mainly provide the interband coupling. We thus set $\lambda_{ii}^{ph} = 0.2$ [4] and $\lambda_{ii}^{sf} = \lambda_{ij}^{ph} = 0$ so that the electron-boson coupling matrix becomes

$$\begin{pmatrix} \lambda^{ph} & \lambda_{12} & \lambda_{13} \\ \lambda_{12}\nu_{12} & \lambda^{ph} & 0 \\ \lambda_{13}\nu_{13} & 0 & \lambda^{ph} \end{pmatrix},$$

where $\nu_{12} = N_1(0)/N_2(0)$ and $\nu_{13} = N_1(0)/N_3(0)$. $N_i(0)$ is the normal density of states at the Fermi level for the ith band, calculated from the first-principles local-density approximation bands of the 8% Co-doped compound [26], first shifted downward in energy and then renormalized by a factor of 2 to agree with the ARPES results [20,27]. To satisfy the conservation of the total charge, the energy shift is 30 meV for the h bands and 46 meV for the e bands. The total density of states of electron bands is then divided in a 4:1 proportion between bands 2 and 3. This is consistent with the Raman data [22] that suggest the existence of "hot spots" (where the gap is strongly suppressed) which occupy about 1/2 or less of one out of two electron pockets [21]. This uneven density of states splitting is very important to obtain a satisfactory agreement between the experimental data and the results of the Eliashberg model. Following the above, $\nu_{12} = 1.12$ and $\nu_{13} = 4.50$. As for the electron-SF spectral function, we used a Lorentzian curve peaked at $\Omega_{ij} = \Omega_0 = 12$ meV, in agreement with neutron scattering experiments [2].

The only two free parameters of the model are λ_{12} and λ_{13}, which are chosen so as to reproduce the experimental gaps as well as possible [11]. The obtained gap values are $\Delta_1 = 6.1$ meV, $\Delta_2 = -3.8$ meV, and $\Delta_3 = -8.0$ meV (with a theoretical $T_c \approx 29.7$ K). Δ_1 (hole FS) and Δ_2 (outer electron FS) are in very good agreement with the ARPES experiments [20], which actually measured the gap only on one of the two electron FS sheets. Also, Δ_2 and Δ_3 are consistent with the gap values observed in our PCAR experiments; resolving the intermediate gap by PCAR is a challenging task. Thus, the whole set of data from ARPES, PCAR, and calculations looks consistent. The coupling constants are $\lambda_{12} = 0.61$ and $\lambda_{13} = 1.22$ corresponding to a total effective coupling constant $\lambda_{eff} = 1.93$, which indicates, as expected, a strong-coupling character for this compound.

Let us now discuss the aforementioned additional structures at about 20 mV that are reproducibly observed in the PCAR spectra (see Fig. 2) and that disappear at the critical temperature of the contacts. We will show here that these structures are the signature of the strong electron-boson coupling, where the boson characteristic energy is the spin-resonance energy observed by neutron scattering. Figure 4(a) shows the normalized conductance at 4.2 K of a ab-plane contact where the AR signal is particularly high ($\approx 30\%$), and the structures at $\sim$20 mV are clearer than usual, which makes this curve particularly interesting for our discussion. The solid line is the theoretical PCAR spectrum obtained from a three-band BTK model by replacing the constant BCS gaps with the energy-dependent gap functions (for details on this procedure, see Sec. 4.3.5 of Ref. [16]) calculated within the same Eliashberg model and with the same parameters discussed above. In the absence of a theoretical way to account for the broadening parameter Γ within the Eliashberg theory, the diffusive normal-metal–superconductor junction model was used to adjust the amplitude of the curve to the experimental one [28] without changing the position or shape of its features. This requires fixing a single parameter $R_d/R_b = 1.015$, where R_d (R_b) is the resistance of the diffusive bank (of the junction). The theoretical AR spectrum clearly shows high-energy structures very similar, in position

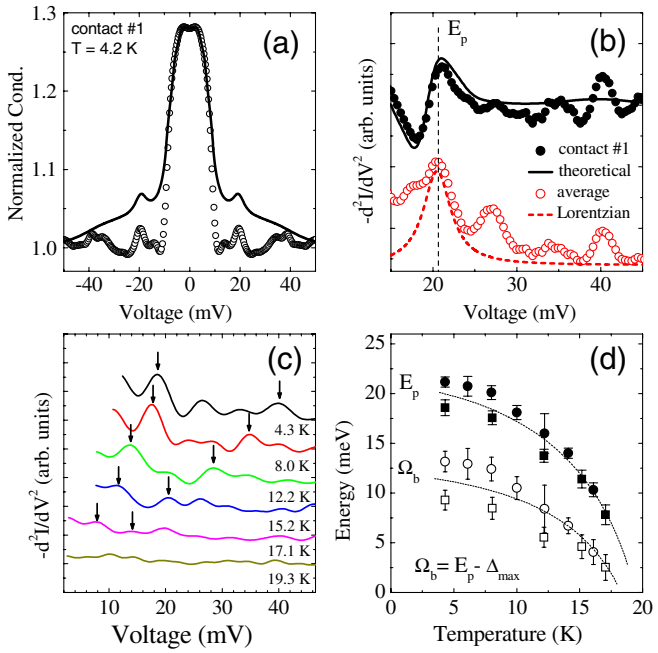

FIG. 4 (color online). (a) An experimental AR spectrum (symbols) compared to the theoretical one (line) obtained from Eliashberg and BTK calculations (see text). (b) Experimental (full symbols) and theoretical (solid line) $-d^2I/dV^2$ vs V curves obtained from the data in (a). Open symbols: The $-d^2I/dV^2$ curve averaged over 5 contacts. Dashed line: The electron-boson spectral function (shifted in energy by $\approx \Delta_{\max}$) used in the three-band Eliashberg calculations. (c) Temperature dependence of the $-d^2I/dV^2$ curves showing the displacement of the bosonic structures. The energy of the peak $E_p(T)$ and the corresponding characteristic boson energy $\Omega_b(T)$ are shown in (d). Lines are guides to the eye.

and in amplitude, to the experimental ones. Figure 4(b) reports the $-d^2I/dV^2$ curve for the experimental (full symbols) and theoretical (solid line) conductance curves shown in Fig. 4(a). In low-transparency (large Z) point contacts on strong-coupling superconductors, peaks in $-d^2I/dV^2$ correspond to peaks in the electron-boson spectral function. In the case of small Z, a small relative shift is observed [16], but here it turns out to be negligible (< 0.2 meV). A peak in the experimental $-d^2I/dV^2$ is clearly visible at about 21 meV (and is observed also in the theoretical curve). Other structures appear around 27 and 40 mV. All these structures exist also in the $-d^2I/dV^2$ curve obtained by averaging over 5 different contacts (open symbols). The energy of the first maximum, E_p, agrees well with the energy of the peak in the Lorentzian electron-boson spectrum used in our calculations, shifted by $\sim\Delta_{\max}$ (dashed line) [16], further indicating that a bosonic mode at Ω_0 is really playing a major role in the coupling. The structures at higher voltage that do not appear in the theoretical $-d^2I/dV^2$ [solid line in Fig. 4(b)] may be due to the actual shape of the electron-SF spectral function and/or to nonlinear strong-coupling effects. Figure 4(c) shows that, on increasing temperature, all the EBI structures shift to lower energy. Figure 4(d) reports the maximum and minimum values of E_p over the different $-d^2I/dV^2$ curves (full symbols) and of the quantity $E_p - \Delta_{\max}$ (open symbols) as a function of temperature. Note that the latter is the energy of the "resonant mode" in the electron-boson spectrum, Ω_b ($\Omega_b \simeq \Omega_0$ at low T) [29] and its behavior is indeed very similar to that of the spin-resonance energy measured by neutron scattering experiments [13].

In conclusion, PCAR measurements give direct and clear evidence for multiband strong-coupling superconductivity in $Ba(Fe_{1-x}Co_x)_2As_2$. They also allow extracting the characteristic energy of the mediating boson and its T dependence, which both coincide with those of the spin resonance measured by neutron scattering experiments [13]. This brings unambiguous evidence for a spin-fluctuation-mediated $s\pm$ mechanism of superconductivity in this compound.

We thank M. Putti for providing the samples and I. I. Mazin and E. Cappelluti for invaluable discussions. This work was done within the PRIN Project No. 2008XWLWF9-005.

*renato.gonnelli@polito.it

[1] Y. Kamihara *et al.*, J. Am. Chem. Soc. **130**, 3296 (2008).
[2] J. Paglione and R. L. Greene, Nature Phys. **6**, 645 (2010).
[3] I. I. Mazin, Nature (London) **464**, 183 (2010).
[4] L. Boeri, O. V. Dolgov, and A. A. Golubov, Phys. Rev. Lett. **101**, 026403 (2008).
[5] Z. A. Ren *et al.*, Europhys. Lett. **83**, 17 002 (2008).
[6] L. Boeri *et al.*, Phys. Rev. B **82**, 020506(R) (2010).
[7] I. I. Mazin *et al.*, Phys. Rev. Lett. **101**, 057003 (2008).
[8] C.-T. Chen *et al.*, Nature Phys. **6**, 260 (2010).
[9] K. Kuroki *et al.*, Phys. Rev. B **79**, 224511 (2009).
[10] J.-Ph. Reid *et al.*, Phys. Rev. B **82**, 064501 (2010).
[11] G. A. Ummarino *et al.*, Phys. Rev. B **80**, 172503 (2009).
[12] L. Benfatto, E. Cappelluti, and C. Castellani, Phys. Rev. B **80**, 214522 (2009).
[13] D. S. Inosov *et al.*, Nature Phys. **6**, 178 (2010).
[14] A. S. Sefat *et al.*, Phys. Rev. Lett. **101**, 117004 (2008).
[15] D. Daghero *et al.*, Phys. Rev. B **80**, 060502(R) (2009).
[16] D. Daghero and R. S. Gonnelli, Supercond. Sci. Technol. **23**, 043001 (2010).
[17] R. S. Gonnelli *et al.*, Phys. Rev. B **79**, 184526 (2009).
[18] P. Szabó *et al.*, Phys. Rev. B **79**, 012503 (2009).
[19] A greater number of bands in the model implies so many free parameters that the fit becomes meaningless.
[20] K. Terashima *et al.*, Proc. Natl. Acad. Sci. U.S.A. **106**, 7330 (2009).
[21] I. I. Mazin *et al.*, Phys. Rev. B **82**, 180502(R) (2010).
[22] B. Muschler *et al.*, Phys. Rev. B **80**, 180510(R) (2009).
[23] P. Vilmercati *et al.*, Phys. Rev. B **79**, 220503(R) (2009).
[24] C. Utfeld *et al.*, Phys. Rev. B **81**, 064509 (2010).
[25] I. I. Mazin and J. Schmalian, Physica (Amsterdam) **469C**, 614 (2009).
[26] I. I. Mazin (private communication).
[27] M. Yi *et al.*, Phys. Rev. B **80**, 024515 (2009).
[28] I. Shigeta *et al.*, J. Phys. Chem. Solids **69**, 3042 (2008).
[29] P. Popovich *et al.*, Phys. Rev. Lett. **105**, 027003 (2010).